AIMS Materials Science, 9(4): 653–667.
DOI: 10.3934/matersci.2022040
Received: 08 March 2022
Revised: 13 June 2022
Accepted: 29 June 2022
Published: 18 August 2022

http://www.aimspress.com/journal/Materials

Research article

Experimental evaluation of additively deposited functionally graded material samples-microscopic and spectroscopic analysis of SS-316L/Co-Cr-Mo alloy

Yakkaluri Pratapa Reddy[1], Kavuluru Lakshmi Narayana[1,*], Mantrala Kedar Mallik[2], Christ Prakash Paul[3] and Ch. Prem Singh[3]

[1] Department of Mechanical Engineering, Koneru Lakshmaiah Education Foundation (KLEF), Green Fields, Vaddeswaram, Guntur Dt-522 302, Andhra Pradesh, India
[2] Department of Mechanical Engineering, Vasireddy Venkatadri Institute of Technology (VVIT), Namburu, Guntur Dt-522 508, Andhra Pradesh, India
[3] Laser Development and Industrial Applications Division, Raja Ramanna Center for Advanced Technology (RRCAT), Indore-452 013, Madhya Pradesh, India

* **Correspondence:** Email: drkln@kluniversity.in; Tel: +91 98493 47580.

Abstract: The gradual and uniform variation in the composition of the material, generally two, is called functionally graded materials (FGM). These FGM are used in practical applications to advantage both material properties. Several methods are used to fabricate the FGM components. The current article is research on the direct energy dispersive technique of 3D Printing employed for depositing the SS316L and Co-Cr-Mo alloy FGM samples. L9 orthogonal array of Taguchi method is used. Process parameters like laser power, powder feed rate and scan speed have been used for deposition. Their structural properties are analysed using scanning electron microscopy, X-ray diffraction, element dispersive technique, and Fourier transform impedance spectroscopy. The results reveal that defect-free samples were deposited, and all the samples have Body Centered Cubic structure except one. Good elemental bonding was observed between SS316L and Co-Cr-Mo alloy.

Keywords: scanning electron microscopy; X-ray diffraction; fourier transform impedance spectroscopy; functionally graded material; laser engineered net shaping

1. Introduction

Japanese Scientists first attempted functionally graded materials (FGM) in the 1980s. These FGMs came into existence due to the failure of conventional materials through delamination at corners in harsh and high-temperature environments. FGMs always deserve their importance through specific properties and are notably used by manufacturers and scientists in various fields. It is a novel composite material where the constituents and compositions gradually vary according to the user-defined design and applications. Due to its gradual variation in material compositions, the FGM possesses enhanced properties than parent materials.

In Additive Manufacturing (AM) process, the material is deposited in the layer-by-layer form in a melt pool route that a laser beam has previously produced. Scientists and researchers in this domain are concerned with the AM process, such as material constraints, process modelling and simulation. Furtherly the post-processing methods were also discussed [1].

The SS-316L/17-4PH combination was used to manufacture FGMs, which are evaluated for microstructure and microhardness using the Laser Metal Deposition (LMD) process. Both microstructure and hardness were altered with depth [2]. TiC/Ti composites varying from pure Ti to approximately 95 volume percentage TiC were developed and evaluated for microstructure and X-ray diffraction (XRD). The results are compared to those of a homogenous composite containing a high TiC concentration. The FGM samples outperform homogeneous composites in crack-free manufacturing and have high hardness [3].

The Direct Energy Deposition (DED) method fabricates Co-Cr-Mo alloys with different laser power and powder feed rates. The samples are characterised for mechanical and metallurgical properties from Scanning Electron Microscopy (SEM) analysis and networked and jagged carbides are observed. The XRD results reveal the presence of γ and ε phases [4]. Laser deposition showed a functionally graded Co-Cr-Mo coating on Ti-6Al-4V substrate varying from 0 to 100%. The thermal expansion of coating materials was controlled by controlling of cooling rates of materials. The absence of a brittle intermetallic phase between Titanium and Cobalt was observed by XRD analysis. Microhardness was observed by the increment of Co-Cr-Mo content [5]. The SS-316L components produced by the Selective Laser Melting (SLM) process are tested for grain structures and found that temperature gradients influenced the crystal development. The high volume of energy density leads to grain size and densification [6].

316L Stainless Steel material samples are fabricated using Laser Engineered Net Shaping (LENS) process and evaluated for different dual-phase microstructures. By increasing the Co-Cr-Mo content and the reduction of Ni was observed. By Schaeffler diagram and Electron Back Scattered Diffraction (EBSD) results in an intercellular delta ferrite on subgrain boundaries and austenite fine grains. Due to LENS deposition, the sigma (FeCr) phases are present in 316L steel [7]. Using the Laser powder bed fusion (LPBF) process, SS-316L coupons are fabricated in different orientations on substrate plate and evaluated for density of pores, tensile testing, Charpy impact testing, microhardness, and microstructure. Results reveal that defects were observed due to a lack of fusing ability, and hardness was the same at all levels [8]. Various fabrication methods of AM and their fabrication techniques to develop complex parts are reviewed by many researchers according to their applications [9]. Laser Metal Deposition (LMD) process fabricates titanium FGM samples added with a varying amount of Molybdenum (Mo). Results exhibit that interfacial bonding between the layers was excellent, and the hardness of the material was reduced as the Mo content increased [10].

By AM process, continuous energy deposition in the z-direction with laser intensity, powder feed rate, and scan speed as process parameters were employed in a novel way to produce 316L thin rods. Various metallurgical and mechanical tests were performed to investigate the impact of process factors and found an excellent dual-phase microstructure of austenite/ferrite with good plastic deformation [11].

A six-layer FGM sample of Ti/TiAl was constructed and deposited on a Ti substrate. The samples are characterised for microstructure, hardness, and phase determination tests. Increasing energy input decreases both the cooling rate and hardness of the FGM samples. Cracks were observed in samples when 100%-TiAl was placed on a pure Ti substrate [12]. Transition path design, fabrication, and characterisation of various parts through the LMD process have been discussed. Model representation and numerical simulation are proposed [13]. Using a laser deposition approach, SS316L-Si combination FGM was produced on an SS-316L base substrate, and a metallurgical connection between the materials was seen by epitaxial nucleation of the columnar grains. Austenite and secondary-ferrite phases were found in the microstructure [14].

The micro to macro grain structure is visible in LENS deposited 316L steel specimens as a function of deformation rates. Twinning deformation was found in hot-forged 316L samples, but dislocation slip caused deformation in LENS deposited materials [15]. Through XRD analysis, a "completely austenitic phase" introduced with residual stresses was identified in SS-316L samples created by laser metal deposition and examined for microstructure-property correlation. The SS-316L alloy has a high hardness and strength compared to as-cast alloys. The lowering of yield and ultimate strength is evaluated by tensile tests [16]. As-built Co-Cr-Mo samples were heat-treated at 1050 ℃ for 2 h. Prior cellular structures were disintegrated when the as-built samples were treated. SEM, EDS, and XRD examinations are used to investigate the characteristics of materials [17]. FGM composed of SS-316L and Inconel-718 was fabricated and studied, and samples were examined for microstructural, defect behaviour, and Vickers hardness (Hv) of the material [18]. Fabrication of FGM with compositionally graded Ni-Co-Cr-Mo alloy was done, and the samples were assessed for tensile and hardness, as well as the creation of distinct phases [19].

Using the Twin wire and arc additive manufacturing (T-WAAM) method, an FGM was fabricated by depositing Cu-based alloy on top of high strength low alloy (HSLA) steel. Due to mixed composition, the samples are evaluated for microscopic analysis and retained δ-ferrite in a Cu-matrix at the interface zone. A gradual gradient of hardness was observed [20].

The impacts of process parameters on build quality (porosity, residual stress, and composition changes) and materials attributes (microstructure and micro segregation) were compared between laser welding and laser-based additive manufacturing. Although this research focuses on laser powder bed fusion, the concepts can be adapted in various ways [21].

18Ni maraging steel samples were manufactured at 802 ℃ homogenised using the SLM technique. Later, they were subjected to isothermal tempering to achieve martensite-to-austenite reversion. Austenite + ferrite field was predicted using thermodynamic calculations [22].

18Ni maraging steel was fabricated by laser-based powder bed fusion, and samples were evaluated for In-situ synchrotron X-ray diffraction. Austenite volume fraction and lattice parameter evolution were retrieved from the austenitic field's physical simulation of continuous heating cycles [23].

The current research uses various characterisation tests to evaluate LENS deposited FGM samples ranging from 100% SS-316L to 100%Co-Cr-Mo alloy. The microscopic analysis was used

to determine the type of crystalline structure generated, surface morphology, phase determination, molecular components, lattice structures, and chemical content of FGM samples.

2. Materials and methods

2.1. Materials

This investigation employed commercially available, gas atomised, spherical-shaped powders of SS-316L and Co-Cr-Mo alloy (Kennametal Inc., USA) powders. Table 1 lists powders' maximum (mass %) elemental compositions from the supplier database. SS-316L has a particle size of 150 µm/50 µm, while Co-Cr-Mo alloy has a particle size of 180 µm/53 µm.

Table 1. Chemical composition of selected powder materials (mass%).

Element	Co	Ni	Cr	W	Mo	C	Fe	Si	B	Others
Co-Cr-Mo alloy	Bal.	2.6	27.5	-	5.4	0.3	-	-	-	-
SS-316L	-	13.0	18.0	-	2.6	-	Bal.	1.8	-	-

Note: -indicates 0% of element content from supplier database.

2.2. Laser engineered net shaping process

In the present work, a LENS machine, Figure 1b, equipped with an Yttrium fibre laser, dual powder feeder, coaxial powder feedstocks, software console and controlled environment chamber is employed to deposit the samples.

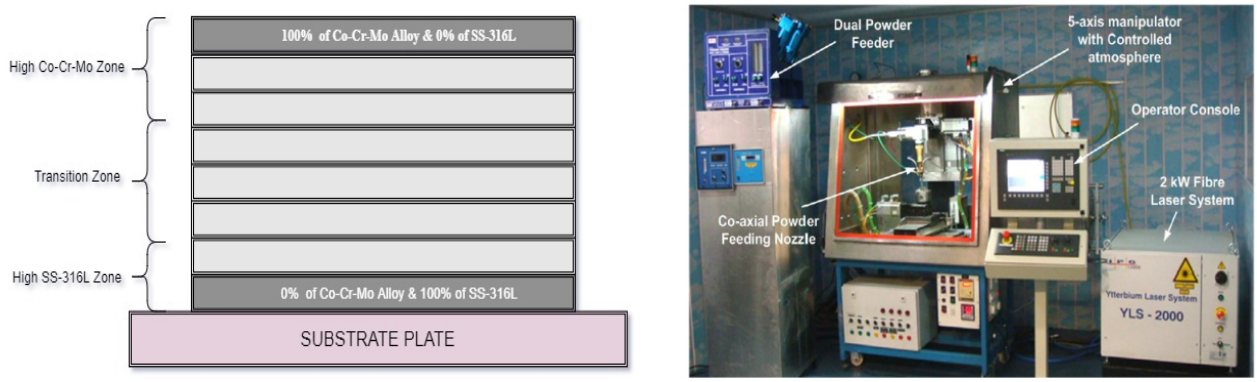

(a) (b)

Figure 1. Details of FGM (a) Schematic diagram of FGM, (b) Laser Additive Manufacturing Machine (Courtesy: RRCAT, Indore, MP.).

The current test samples are deposited with the LENS process using the process parameters listed in Table 2, designed by the Taguchi method's L9 Orthogonal Array (OA) method. The samples are deposited as 60 × 10 × 10 mm^3 sizes on the substrate plate using the preset process parameters as factors, each at three levels. The surface of the substrate plate is ground with Silicon Oxide (SiO_2)

emery papers before the deposition process begins (grit size 600, 800 and 1000). The substrate surface is cleaned using acetone to eliminate dust and foreign particles. The sample deposition process is carried out in an Argon-gas-controlled atmosphere to keep the oxygen (O_2) level below 10 ppm and prevent the samples from oxidising.

Table 2. L9 Orthogonal Array of LENS process parameters.

Set/sample No.	Laser power (LP) (watts)	Powder feed rate (PFR) (g/min)	Scan speed (SS) (m/min)
S-1	800	6	0.4
S-2	800	9	0.5
S-3	800	12	0.6
S-4	1000	6	0.5
S-5	1000	9	0.6
S-6	1000	12	0.4
S-7	1200	6	0.6
S-8	1200	9	0.4
S-9	1200	12	0.5

The material deposition (first layer of deposition on the substrate plate) begins with 100 percent SS-316L and gradually increases the amount of Co-Cr-Mo alloy in succeeding layers. Finally, the CAD design specifies that the sample is finished with a 100% Co-Cr-Mo alloy top layer. The FGM schematic diagram is provided in Figure 1a, and the laser deposition machine is illustrated in Figure 1b. The as-deposited sample on the LENS machine is shown in Figure 2a, and the polished sample is presented in Figure 2b.

A piece of the sample (about 5 mm) is carved from the transition zone for the current study analysis using the Wire Electrical Discharge Machining (Make: Electronica, Model: 1-Enova-1S, India) technique. Before testing, all samples' surfaces are polished with a disc polishing machine and with emery papers of grit size 600, 800 and 1000, respectively, according to the standard process for achieving a smooth surface and etched with a 5% aqueous solution of HCl (50 mL of HCl added with one litre of H_2O).

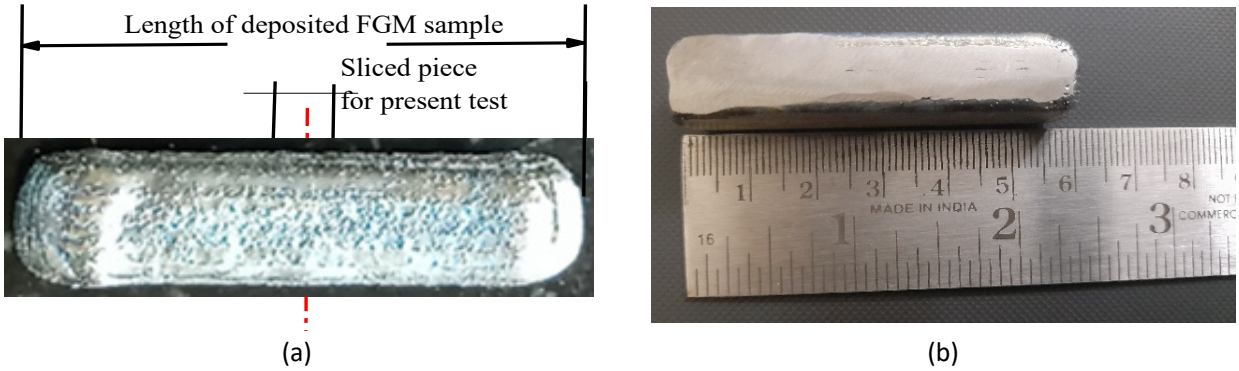

Figure 2. Details of LENS deposited sample (a) as deposited before grinding and polishing, (b) actual sample length after grinding and polishing.

2.3. Testing

A scanning electron microscope is used to examine the surface morphology of LENS-deposited FGM samples (model: VEGA-3, TESCAN, Czech Republic). The FGM sample is examined at a high voltage of 10 kV, at a magnification of 500× at 100 m, and with Photoelectron Diffraction (PD) at a lower level of 4.02 keV and a higher level of 11.27 keV, where a high beam of electrons is employed as a columnar probe. The reflection of deflected secondary electrons from the sample surface generates an image.

An X-ray Diffractometer (Make: PANalytical, Model: EMPYREAN) using Copper (Cu) as anode material is utilised to perform a phase test on the FGM sample at wavelengths ranging from K = 1.5405980 to K = 1.5444260. The diffractograms are displayed as a function of intensity (a.u.) and 2θ angle (in degrees). The high peak intensities acquired from the plots are examined with X'Pert High-score software to reveal the miller indices, planes (hkl), and crystalline structure.

The FGM samples are then subjected to a Fourier Transform Infrared Spectroscopy (FTIR) examination at an incidence angle of 45º. The test parameters for the current investigation are a conventional light source, a GS detector with a resolution of 4 cm^{-1}, and a scanning speed of 2 mm/s. For each of the nine samples, the IR spectra are displayed between wave number (cm^{-1}) on the x-axis and percentage transmittance (% T) on the y-axis.

Finally, the FGM samples were subjected to an Energy Dispersive X-ray spectroscopic (EDS/EDAX) analysis to establish the element type, atomic %, and chemical composition. The investigation comprises element dispersion caused by the influence of specified process factors during deposition. The EAX detector with C2-element captures the energy-dispersive spectrum at a −34º angle and a beam intensity of −10 kV.

3. Results and discussion

The results obtained from the tests conducted on LENS deposited FGM samples are listed and discussed below.

3.1. Scanning electron microscopy (SEM)

The SEM pictures in Figure 3 show that the Set-1 sample (Figure 3a) deposited with LP-800 watts, PFR-6 g/min, and SS-0.4 m/min reveals a few refulgent particles caused by precipitation following particle solidification. Furthermore, due to divergence in process parameters, a progressive increase in these dazzling luster particles was detected from Figure 3a to Figure 3i. According to Figure 3i, the increase in process parameters created a heap of these dazzling particles, but they are disseminated throughout the surface by the action of scan speed during deposition. Figure 3j (Set-8) depicts the formation of parallel and columnar dendrites as deposited with a laser power of 1200 watts, powder feed rate of 9 g/min, and a scan speed of 0.6 m/s at a rich Co-Cr-Mo zone, which was presumably caused by rapid cooling and abrupt descent in temperature at the interface zone due to precipitation caused by the solidification process. This notion shows that the direction of heat transfer is parallel to the surface of the substrate plate. Columnar dendrites are always formed in the opposing direction of heat flow. The Set-9 sample, Figure 3k, exhibits a tailed and acicular dendritic structure after being deposited with a laser power of 1200 watts, a powder feed

rate of 12 g/min, and a scan speed of 0.5 m/s. These dendrites are most likely formed in Fe-based alloys due to an uneven solidification process across different phases.

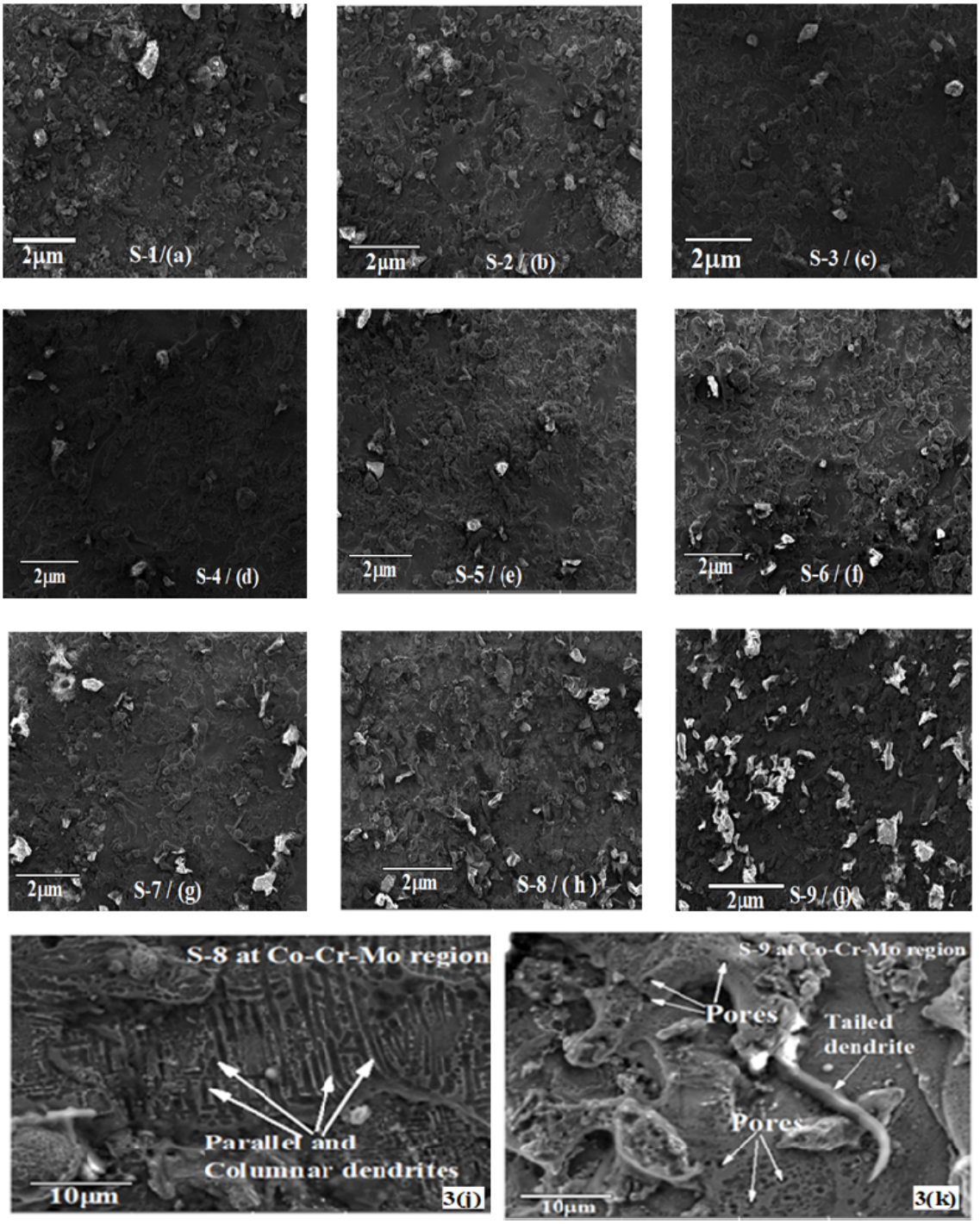

Figure 3. SEM micrographs of FGM samples.

3.2. X-ray diffraction (XRD)

The phase and crystallinity of LENS deposited FGM samples are investigated using X-ray diffraction (Figure 4) by employing Hermann-space Mauguin's grouping technique and a threefold

symmetry of the body diagonals. The crystal structure is evaluated as cubic for all nine sets of samples using X'Pert High Score software, and it is discovered that they are lying in a space group of "Pm3m" and "Fd3m" with primitive group mirror planes and a lattice type of "P" as determined by an XRD diffractogram. The second sample (Set-2) has a hexagonal-shaped crystal structure with a space group of "P63/mmc". The sample is deposited at LP-800 watts, PFR-9 g/min, and SS-0.5 m/min.

The miller indices values and reference COD numbers generated by assessing the diffractogram curves using the X'Pert High Score software attached to the XRD instrument are shown. In X'Pert High score software, a "search and match" algorithm is used to compare the empirically recorded pattern to the standard pattern, which specifies the phase formed during FGM sample deposition. In Figure 4, peak intensities were observed in all samples, showing that they are all crystalline.

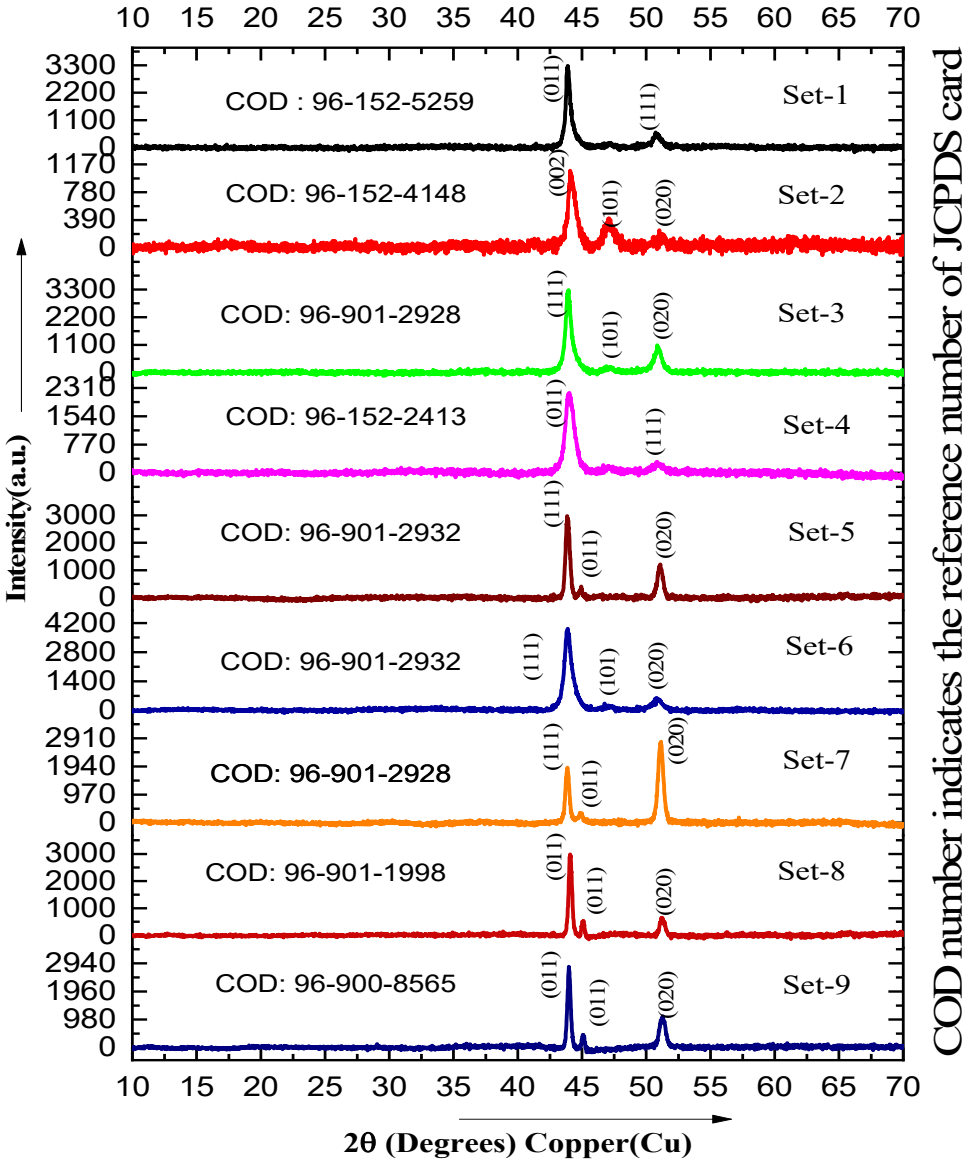

Figure 4. XRD diffractograms of FGM samples (COD Number indicates the reference number of the JCPDS card).

XRD results show that all investigated samples (from S-1 to S-9) have a "cubic" crystal structure, apart from sample S-2, which has unit cell values listed in Table 3. The sample S-2, on the other hand, has a "hexagonal" crystal structure with unit cell values of a = b ≠ c and α = β = 90º, γ = 120º and belongs to the space group ($P6_3/mmc$). The letter "P" represents the primitive group, the first letter "m" indicates the mirror plane perpendicular to the c-axis, the second "m" indicates the mirror plane parallel to the c-axis, and "c" works as a glide plane to "b" and "c", as these space groups have a "centrosymmetric" point of inversion.

Table 3. Details of Crystal shape and space group (with ref. to JCPDS card).

Set No.	Reference number of JCPDS Card	Crystal shape obtained by XRD test	Unit-cell geometry	Space group
1	COD:96-152-5259	Cubic	a = b = c and α = β = γ = 90º	Pm3m
2	COD:96-152-4148	Hexagonal	a = b ≠ c and α = β = 90º, γ = 120º	$P6_3/mmc$
3	COD:96-901-2928	Cubic	a = b = c and α = β = γ = 90º	Fm3m
4	COD:96-152-2413	Cubic	a = b = c and α = β = γ = 90º	Pm3m
5	COD:96-901-2932	Cubic	a = b = c and α = β = γ = 90º	Fm3m
6	COD:96-901-2932	Cubic	a = b = c and α = β = γ = 90º	Fm3m
7	COD:96-901-2928	Cubic	a = b = c and α = β = γ = 90º	Fm3m
8	COD:96-901-1998	Cubic	a = b = c and α = β = γ = 90º	Fd3m
9	COD:96-900-8565	Cubic	a = b = c and α = β = γ = 90º	Fd3m

3.3. Fourier transform infrared spectroscopy (FTIR)

As shown in Figure 5, all the samples (from S-1 to S-9) exhibit the same infrared spectral pattern based on Fourier Transform IR Analysis. The fingerprint region has low transmittance (wave number 500–1600 cm^{-1}), and all samples have a larger percentage of transmittance from wave number 3500–4000 cm^{-1}, which has several high-intensity peaks and endures stretching and bending vibrations of molecules. When all spectrums are compared, the deviation is noticed at the wave number from 2200–2300 cm^{-1}, where the spectrum gradually enhances in size and becomes a wide pattern from S-1 to S-9. This is due to the increment of Co-Cr-Mo content in the sample (as the Co-Cr-Mo is gradually increased from 0 to 100% from S-1 to S-9 sample during deposition) because the tested samples are taken at the middle part of each sample. This may be caused by creating hydrogen (H) bonds or a shift in polarity between atoms, particularly in a functional group area. The smallest peaks (wave number (1750–3500 cm^{-1}) suggest that the molecule in this zone has a very low percentage of light transmittance (%T). This is most noticeable at the transition zone for all samples, owing to a dense population of bonds and substantial absorption of the incident light, resulting in a low transmittance wavelength. One of the causes for the decreased % transmission of light from molecules could be the strong bonding (such as a triple bond) between molecules. Only stretching vibrations from wave numbers 3000–4000 cm^{-1} in Figure 6 exhibit numerous intensities in this sort of strong bonding.

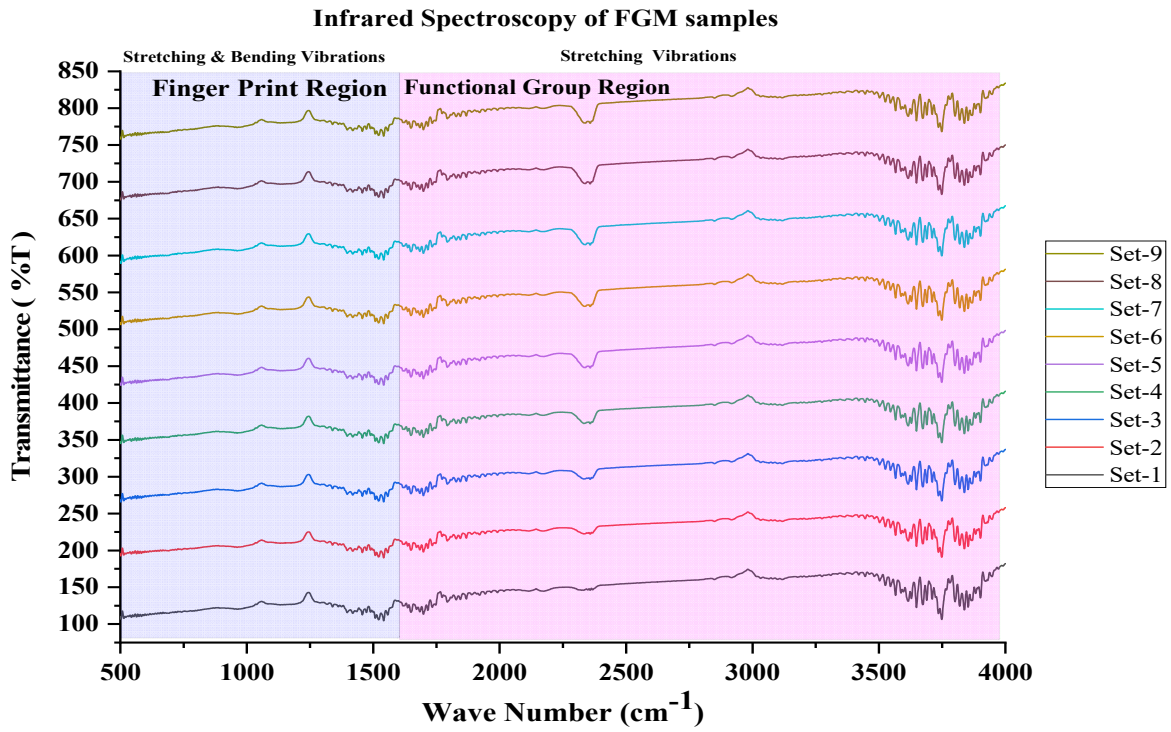

Figure 5. Infrared Spectroscopy of FGM samples.

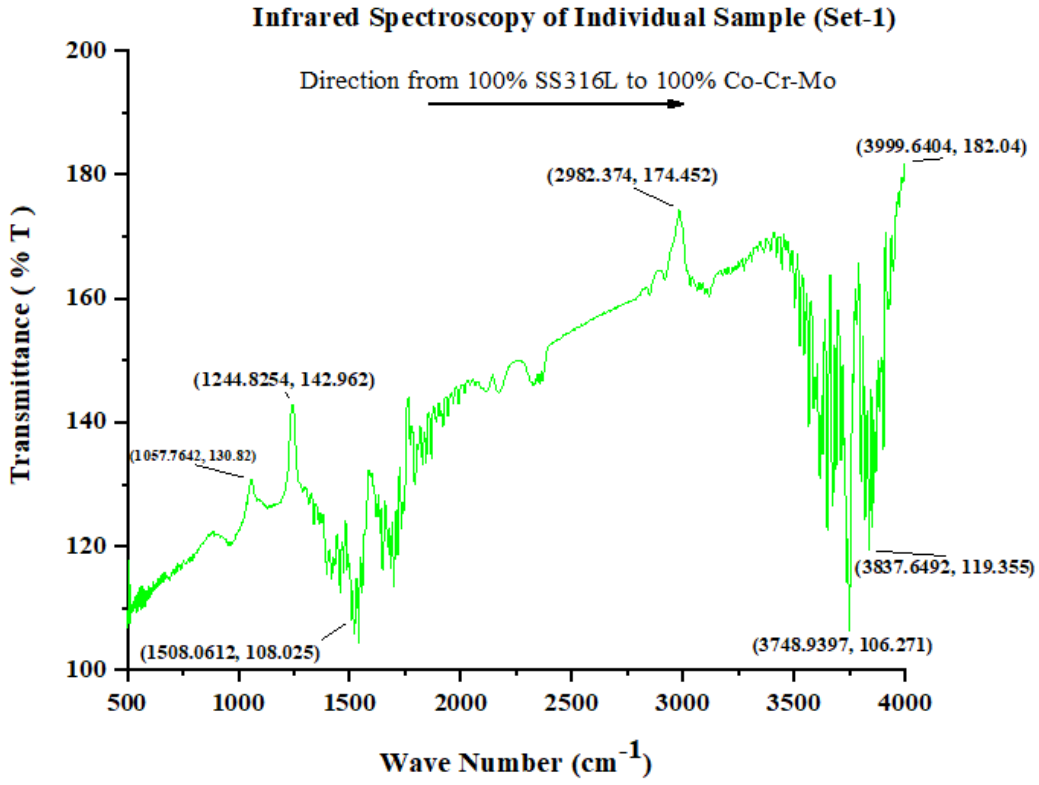

Figure 6. Infrared Spectroscopy of individual sample/Set-1.

3.4. Energy-dispersive X-ray spectroscopy (EDS)

In EDS analysis, three randomly selected samples are examined by EDS spectra at two places on FGM samples to evaluate the dispersion of elements induced by the influence of process parameters, as illustrated in Figure 7a–c. According to the findings, the primary constituents in various zones include Fe, Co, Cr, Ni, and Mo. According to Figure 7a, the same type of spectra was seen for all three sets of samples, with the only difference being the existence of elements and their weight percentage. The iron (Fe) content in set-1 (S-1) at the SS-316L zone is moderate (15.53 wt%); however, the presence of Chromium (Cr) is less (4.46%), and Cobalt is 0.02%. But the percentage of iron (Fe) in the Co-Cr-Mo zone is only 5.07% by weight, Co is 3.15%, and Cr is 15.65%.

EDS spectra exhibit oxygen (O_2) plays an important role during sample deposition, with a high peak intensity. All the samples have the same distribution of chromium particles. The iron (Fe) element exhibits and confirms that when the error (55.64%) is high, it infers the weight (1.72%) is less, which is deposited with a moderate laser power of 1000 watts. The penetration of Cobalt chromium particles is observed from EDS spectra in Figure 7b of the Co-Cr-Mo zone. When the laser power is increased, the oxygen diverges from 8.67 to 8.27%, causing micro-level pores to form in the Co-Cr-Mo area due to entrapped gas content. As the porosity increases, so does the percentage inaccuracy, indicating that the region has a small amount of element content.

The mapping of elements was examined by applying the EDS (mapping) technique, which is associated with the SEM apparatus. Figure 8 illustrates the mapping of all elements at the tested site in the current investigation, emphasising the existence of diverse types of elements (C 10%; O_2 30%; Fe 9%; Co 14%; Ni 9%; Zn 6%; Na 3%; Si 7%; Mo 4% and Cr 8%). This EDS study shows the role of oxygen during sample deposition in a controlled atmosphere, where it occupies the largest percentage (30%), and the element Sodium (Na) exhibits the lowest percentage (3%) of its existence at the measured site.

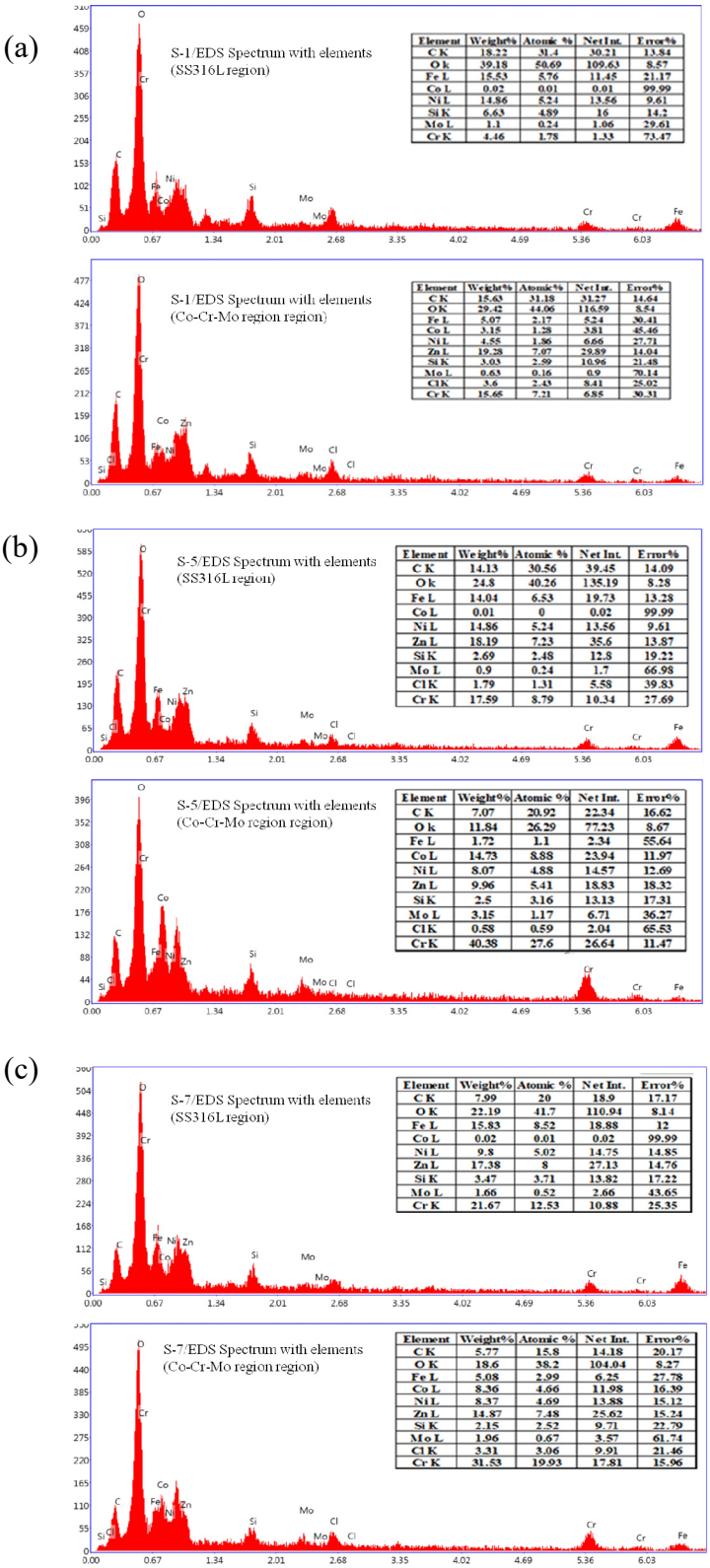

Figure 7. EDS spectrum of FGM samples. (a) Laser power-800 watts, powder feed rate-6 g/min, and Scan speed-0.4 m/min; (b) Laser power-1000 watts, powder feed rate-6 g/min, and Scan speed-0.5 m/min; (c) Laser power-1200 watts, powder feed rate-6 g/min, and Scan speed-0.6 m/min.

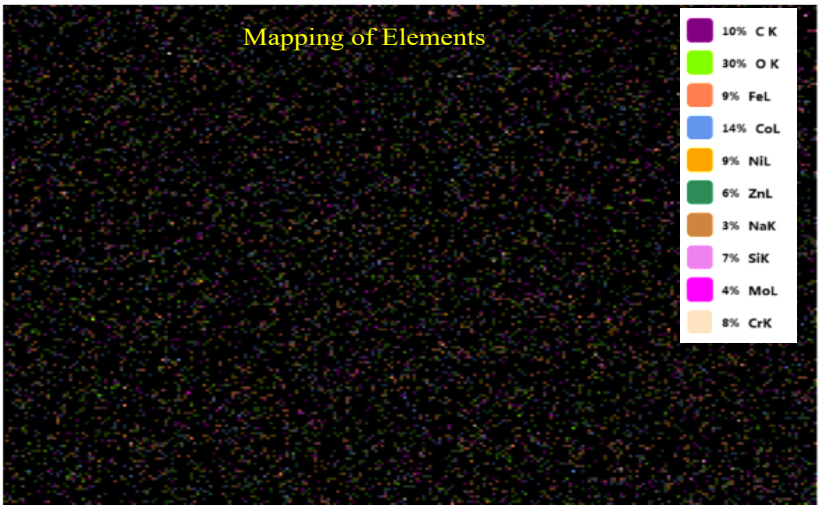

Figure 8. EDX Mapping of all elements in FGM sample.

4. Conclusions

From the present work, the following important conclusions are derived.

(1) In the present work, the LENS deposited FGM samples were subjected to SEM, XRD, FTIR, and EDS analysis to determine the effect of process parameters on sample deposition. The surface morphology, chemical composition, bonding in various fingerprint and functional regions, and dispersion of elements were studied during the deposition of FGM samples.

(2) Columnar, tailed dendrites and infinitesimal pores were observed in the rich Co-Cr-Mo region by the increment of laser power where the precipitation of particles is detected following the solidification process.

(3) The formation of micro-size pores resulted from the entrapment of gas (oxygen) during the solidification process, which cannot escape due to shielded argon gas's presence.

(4) The cubic crystal structure is formed during deposition of samples by the LENS process in a space group of Pm3m/Fm3m with a primitive "P" group, which is evaluated by comparing the obtained experimental diffractogram to standard diffractogram with referred JCPDS/COD card.

(5) In the fingerprint region, the samples exhibit multiple high peak intensities from 3500 to 4000 cm^{-1} wavelength, indicating the formation of triple bonding between molecules and possibly due to a change in polarity between atoms. The molecules undergo the stretching of atoms by the absorbance of light.

(6) A higher population of bonds is one of the reasons for the low percentage of transmittance of light. A gradual increment of broad-spectrum is observed from Set-1 to Set-9 at the functional group region between the wavelength of 2250 to 2500 cm^{-1} by the increment of process parameters.

(7) EDX analysis confirmed that the elements are properly dispersed, and Cobalt has a 99.99% error in the SS-316L rich zone.

(8) This research confirms that FGM material developed by the LENS process exhibits optimistic features, with improved properties suitable for different applications in various fields of science and technology.

Acknowledgements

The authors convey their gratitude to the Department of Science and Technology (DST), Government of India, for sponsoring the equipment in Material Testing Laboratory, K L Deemed to be University, under project vide no: SEED/TIDE/2018/33/G.

Conflict of interest

The authors declare that they have "no" known competing for financial interests or personal relationships that could have appeared to influence the work reported in this paper.

References

1. Zhang C, Chen F, Huang Z, et al. (2019) Additive manufacturing of functionally graded materials: A review. *Mater Sci Eng A-Struct* 764: 138209. https://doi.org/10.1016/j.msea.2019.138209
2. Bayode A, Akinlabi ET, Pityana SL (2019) Fabrication of stainless steel based FGM by laser metal deposition, In: Kumar K, Davim JP, *Hierarchical Composite Materials: Materials, Manufacturing, Engineering*, Berlin, Boston: De Gruyter. https://doi.org/10.1515/9783110545104-004
3. Liu W, DuPont JN (2003) Fabrication of functionally graded TiC/Ti composites by laser engineered net shaping. *Scripta Mater* 48: 1337–1342. https://doi.org/10.1016/S1359-6462(03)00020-4
4. Liu M, Kuttolamadom M (2021) Characterisation of Co-Cr-Mo-alloys via Direct Energy Deposition. *International Manufacturing Science and Engineering Conference*, American Society of Mechanical Engineers, 85062: V001T01A027. https://doi.org/10.1115/MSEC2021-64111
5. Wilson JM, Jones N, Li J, et al. (2013) Laser deposited coatings of Co-Cr-Mo onto Ti-6Al-4V and SS-316L substrates for biomedical applications. *J Biomed Mater Res B* 101: 1124–1132. https://doi.org/10.1002/jbm.b.32921
6. Wang D, Song C, Yang Y, et al. (2016) Investigation of crystal growth mechanism during selective laser melting and mechanical property characterisation of 316L stainless steel parts. *Mater Design* 100: 291–299. https://doi.org/10.1016/j.matdes.2016.03.111
7. Ziętala M, Durejko T, Polański M, et al. (2016) The microstructure, mechanical properties and corrosion resistance of 316 L stainless steel fabricated using laser engineered net shaping. *Mater Sci Eng A-Struct* 677: 1–10. https://doi.org/10.1016/j.msea.2016.09.028
8. Eriksson P (2018) Evaluation of mechanical and microstructural properties for laser powder-bed fusion 316L.
9. Owoputi AO, Inambao FL, Ebhota WS (2018) A review of functionally graded materials: Fabrication processes and applications. *IJAER* 13: 16141–16151.
10. Akinlabi SA, Mashinini MP, Ajayi OO, et al. (2018) Characterisation of laser metal deposited Titanium and molybdenum composite. *IOP Conf Ser Mater Sci Eng* 413: 012067. https://doi.org/10.1088/1757-899X/413/1/012067

11. Weng F, Gao S, Jiang J, et al. (2019) A novel strategy to fabricate thin 316L stainless steel rods by continuous directed energy deposition in Z direction. *Addit Manuf* 27: 474–481. https://doi.org/10.1016/j.addma.2019.03.024
12. Chen X, Yan L, Newkirk JW, et al. (2020) Design and fabrication of functionally graded material from Ti to γ-TiAl by laser metal deposition, *Proceedings of the 28th Annual International Solid Freeform Fabrication Symposium*, 148–159.
13. Yan L, Chen Y, Liou F (2020) Additive manufacturing of functionally graded metallic materials using laser metal deposition. *Addit Manuf* 31: 1–26. https://doi.org/10.1016/j.addma.2019.100901
14. Belsvik MA, Tucho WM, Hansen V (2020) Microstructural studies of direct-laser-deposited stainless steel 316L-Si on 316L base material. *SN Appl Sci* 2: 1–15. https://doi.org/10.1007/s42452-020-03530-3
15. Ziętala M, Durejko T, Panowicz R, et al. (2020) Microstructure evolution of 316L steel prepared with the use of additive and conventional methods and subjected to dynamic loads: A comparative study. *Materials* 13: 4893. https://doi.org/10.3390/ma13214893
16. Nath P, Nanda D, Dinda GP, et al. (2021) Assessment of microstructural evolution and mechanical properties of laser metal deposited 316L stainless steel. *J Mater Eng Perform* 30: 6996–7006. https://doi.org/10.1007/s11665-021-06101-8
17. da Silva Costa AM, Oliveira JP, Munhoz ALJ, et al. (2021) Co-Cr-Mo alloy fabricated by laser powder bed fusion process: Grain structure, defect formation, and mechanical properties. *Int J Adv Manuf Technol* 116: 2387–2399. https://doi.org/10.1007/s00170-021-07570-w
18. Kim SH, Lee H, Yeon SM, et al. (2021) Selective compositional range exclusion via directed energy deposition to produce a defect-free Inconel 718/SS 316L functionally graded material. *Addit Manuf* 47: 102288. https://doi.org/10.1016/j.addma.2021.102288
19. Wen Y, Zhang B, Narayan RL, et al. (2021) Laser powder bed fusion of compositionally graded CoCrMo-Inconel 718. *Addit Manuf* 40: 101926. https://doi.org/10.1016/j.addma.2021.101926
20. Rodrigues TA, Bairrão N, Farias FWC, et al. (2022) Steel-copper functionally graded material produced by twin-wire and arc additive manufacturing (T-WAAM). *Mater Design* 213: 110270. https://doi.org/10.1016/j.matdes.2021.110270
21. Oliveira JP, LaLonde AD, Ma J (2020) Processing parameters in laser powder bed fusion metal additive manufacturing. *Mater Design* 193: 108762. https://doi.org/10.1016/j.matdes.2020.108762
22. Conde FF, Escobar JD, Oliveira JP, et al. (2019) Austenite reversion kinetics and stability during tempering of an additively manufactured maraging 300 steel. *Addit Manuf* 29: 100804. https://doi.org/10.1016/j.addma.2019.100804
23. Conde FF, Avila JA, Oliveira JP, et al. (2021) Effect of the as-built microstructure on the martensite to austenite transformation in an 18Ni maraging steel after laser-based powder bed fusion. *Addit Manuf* 46: 102122. https://doi.org/10.1016/j.addma.2021.102122

AIMS Press